Fourth International Symposium on Marine Propulsors
smp'15, Austin, Texas, USA, June 2015

Analysis of Marine Propulsor in Crashback using Large Eddy Simulation

Praveen Kumar[1], Krishnan Mahesh[2]

[1,2] Department of Aerospace Engineering and Mechanics
The University of Minnesota, Minneapolis, MN 55455, USA

ABSTRACT

Dynamic Mode Decomposition (DMD) has been used in recent years to study a variety of canonical flow problems. Each DMD mode corresponds to a single frequency and hence, provides a means to describe dynamics of a complex system. Verma et al. (2012) performed Large Eddy Simulation (LES) at advance ratio, J=-0.5 and J=-1.0 and reproduced the experimentally observed behavior of increase in side-force below J=-0.7 (Bridges, 2004). They examined the effect of hull and explained that in the presence of an upstream hull, there exists a recirculation zone and the ring vortex lies closer to the propeller for highly negative advance ratio leading to higher side-force. In the present work, the complex flow over hull-attached propeller in crashback is analyzed using DMD. DMD of the three-dimensional flow fields is performed to identify dominant frequencies at J=-1.0 and J=-0.5. The corresponding flow features and their relation to the unsteady loads experienced by the hull-attached propeller in crashback are discussed.

Keywords

Large eddy simulation, propulsor, crashback, hull, dynamic mode decomposition, reduced-order model.

1 INTRODUCTION

Crashback is an extreme off-design operating condition in which the vessel moves in the forward direction while the propulsor rotates in the reverse direction. The flow in crashback is highly unsteady and massively separated which makes it computationally challenging. It is important to study as the highly unsteady loads can damage the structure of the propulsor blades and also affect its performance. The highly unsteady side-forces affect the maneuverability of the vessel during crashback.

The crashback condition is dominated by the interaction of the freestream with the strong reverse flow from propulsor rotation as shown in Figure 1. This interaction forms an unsteady ring vortex which is a unique feature of the flow in crashback.

Jiang et al. (1997) used Particle Image Velocimetry (PIV) measurements to study the structure of the unsteady vortex ring. They found that the unsteady vortex ring is related to unsteady shaft forces and the oscillation frequency of the ring vortex is much lower than the propulsor rotation rate. Jessup et al. (2004) presented more detailed measurements of flow velocity fields using PIV and Laser Doppler Velocimetry (LDV).

The computational prediction of the flow around marine propulsors has traditionally been performed using unsteady Reynolds-Averaged Navier-Stokes equations (RANS) (Chen & Stern, 1999; Davoudzadeh et al., 1997). They showed that RANS yielded good results for forward (U>0, n>0) and backward (U<0, n<0) modes, but produced significant discrepancies in crashback (U>0, n<0) and crashahead (U<0, n>0) modes where flow is massively separated. Here, U is the velocity of marine vessel and n is the rotational speed of the propulsor.

A cylindrical cross-section of a propulsor blade resembles an airfoil. In the crashback condition, the leading and trailing edges of propulsor blades exchange their roles. The sharp trailing edge of normal conditions becomes the leading edge. A large flow separation can occur at this sharp leading edge. which may cause high amplitude fluctuation of unsteady loads. Since RANS is based on time or ensemble average, it is unable to accurately predict highly fluctuating loads which occur in crashback. Large Eddy Simulation (LES) is therefore an attractive computational methodology for predicting the flow in propulsor crashback.

Vyšohlíd & Mahesh (2006) performed numerical simulations of crashback condition with LES on unstructured grids at an advance ratio J=-0.7 using the non-dissipative and robust finite volume method developed by Mahesh et al (2004). They showed that LES could yield good results for mean and r.m.s. values of unsteady loads. The computed power spectral density (PSD) for unsteady loads showed the same peak as the experiment at 5 rev^{-1}. Jang & Mahesh (2010) introduced two quantities for pressure contributions to thrust and side-force to give a clearer understanding about the origin of thrust and side-force. They also used conditional averaging to study the flow field. Chang et al. (2008) performed LES with the same LES code and computational grid as Vyšohlíd & Mahesh (2006) but at other advance ratios, J=-0.5 and J=-1.0.

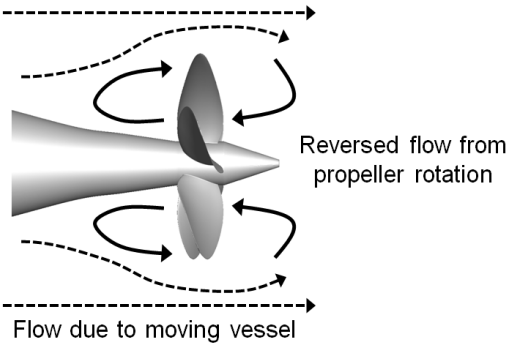

Figure 1. Schematic of crashback condition (Fig. reproduced with permission from Verma et al. 2012).

They investigated instantaneous flow fields at high and low thrust events to understand the physics of crashback. They reported that a bi-modal behavior with vortex ring and axial jet modes occur at low negative J. At high negative J, the flow only acts in ring vortex mode.

Bridges' experiment (Bridges 2004) noted that the side-forces increased dramatically below an advance ratio of J=-0.7 compared to Jessup's experiments (Jessup et al. 2006) when the hull is present (Figure 2). Verma et al (2012) explained the reason for increased side-force below J=-0.7. They performed LES of flow over propeller in crashback with and without hull to examine the effect of hull at advance ratio of J=-1.0 and J=-0.5. They concluded that in the presence of an upstream hull, there exists a recirculation zone and the ring vortex lies closer to the propeller for highly negative advance ratio leading to higher side-force. In contrast, at lower negative advance ratio, there is much smaller recirculation zone which is further upstream due to increased reverse flow. Hence, hull does not make much difference close to the propulsor. They used an axisymmetric hull (DTMB 5495-3) attached to propeller P4381.

The analysis of complex turbulent flow is very challenging because of wide range of scales in both time and space. Crashback is an example of one such flow. The usual way to analyze the flow structures is by decomposing them into modes. Proper Orthogonal Decomposition (POD) and Dynamic Mode Decomposition are two of the most popular techniques used in literature for this purpose. DMD extracts the dominant flow features from the snapshot basis by approximating the linear mapping between snapshots and detecting the pertinent frequencies. It is capable of identifying dynamics of flow features directly from the flow unlike Proper Orthogonal Decomposition (POD), which uses second-order statistics of the flow field (Holmes, Lumley & Berkooz 1996). Each DMD (Koopman) mode contains one particular frequency and hence it is more effective at isolating various dynamics in a complex system, unlike modes obtained from POD which has many frequencies. DMD has been shown to provide accurate and complete description of

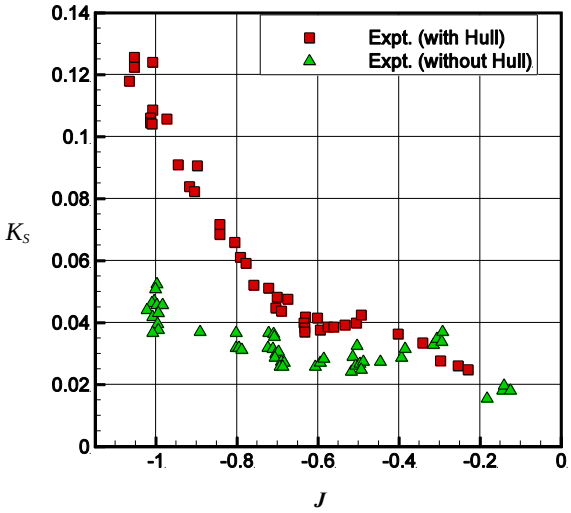

Figure 2. Increase in side-force below J=-0.7 in the presence of hull (Jessup et al. 2006). (Fig. reproduced with permission from Verma et al. 2012).

the flow behavior (Rowley et al. 2009; Schmid, 2010; Bagheri 2013). Mezić (2013) provides a comprehensive review of the use of Koopman modes in the analysis of fluid flows.

Beyond identifying the coherent flow structures, these modes can also be used to obtain low-order models by projecting the full system onto the subspace spanned by the extracted modes. By doing so, the governing equations are approximated by a dynamical system with fewer number of degree of freedom. Such reduced-order model which captures the dominant features of a complex flow system, can be very useful as it facilitates computationally cheap study of the flow behavior including its stability and receptivity. A reduced-order model which captures the essential dynamics of a complex system, can be used for model-based control design.

In the present work, flow over marine propulsor with an upstream hull in crashback is analyzed at two different advance ratios of J=-1.0 and J=-0.5. These advance ratios lie on either side of the critical advance ratio of J=-0.7 beyond which the presence of hull drastically increases the side force magnitude (Figure 2) as mentioned by Bridges (2004). The objectives of the present work are to: (1) identify the dominant frequencies using DMD of the flow field and (2) analyze the flow physics.

This paper is organized as follows. The set-up of the simulation, including the numerical method, grid and boundary conditions, is given in Section 2. A brief description of the DMD algorithm is given in Section 3 followed by discussion of results in Section 4. The paper is summarized in Section 5.

2 SIMULATION DETAILS

2.1 Numerical Method

In LES, the large scale motions are resolved, whereas effects of small scale motions are modeled. Here, simulations are performed in a frame of reference that rotates with the propulsor. The spatially filtered incompressible Navier-Stokes equations are formulated in a rotating frame of reference where the absolute velocity vector is written in inertial frame as follows:

$$\frac{\partial \overline{u_i}}{\partial t} + \frac{\partial}{\partial x_j}(\overline{u_i u_j} - \overline{u_i}\varepsilon_{jkl}\omega_k x_l) = -\frac{\partial \overline{p}}{\partial x_i} - \varepsilon_{ijk}\omega_j \overline{u_k} + \nu \frac{\partial^2 \overline{u_i}}{\partial x_j \partial x_j} - \frac{\partial \tau_{ij}}{\partial x_j} \quad (1)$$

$$\frac{\partial \overline{u_i}}{\partial x_i} = 0$$

with the approximation $\overline{u_i \varepsilon_{jkl}\omega_k x_l} \approx \overline{u_i}\varepsilon_{jkl}\omega_k x_l$.

u_i are the inertial velocities in the stationary frame, p is the pressure, x_i are coordinates in the rotating non-inertial reference frame, ω_j is the angular velocity of the rotating frame of reference, ν is the kinematic viscosity, ε_{ijk} denotes the permutation symbol for the tensor notation, the overbar ($\overline{\ }$) denotes the spatial filter, $\tau_{ij} = \overline{u_i u_j} - \overline{u_i}\overline{u_j}$ is the sub-grid stress. The sub-grid stress is modeled by the dynamic Smagorinsky model (Germano et al., 1991; Lilly, 1992).

Equation (1) is solved by a numerical method developed by Mahesh et al. (2004) for incompressible flows on unstructured grids. The algorithm is derived to be robust without any numerical dissipation. It is a finite volume approach which stores the Cartesian velocities and the pressure at the centroids of the cells and the face normal velocities are stored independently at the centroids of the faces. A predictor-corrector approach is used. The predicted velocities at the control volume centroids are first obtained and then interpolated to obtain the face normal velocities. The predicted face normal velocity is projected so that continuity is discretely satisfied. This yields a Poisson equation for pressure which is solved iteratively using a multigrid approach. The pressure field is used to update the Cartesian control volume velocities using a least-squared formulation. Time advancement is performed using an implicit Crank-Nicholson scheme. The algorithm has been validated for a variety of problems over a range of Reynolds numbers (Mahesh et al., 2004).

2.2 Propulsor Geometry, Computational Mesh and Boundary Conditions

Simulations are performed for a marine propulsor P4381, which is a five-bladed, right-handed with variable pitch and no skew and no rake. The propulsor has been used in various experiments (Jiang et al., 1997; Jessup et al., 2004; Jessup et al., 2006) and computations (Davoudzadeh et al., 1997; Chen & Stern, 1999; Vyšohlíd & Mahesh, 2006; Chang et al., 2008; Jang & Mahesh, 2013; Verma et al., 2012). The detailed

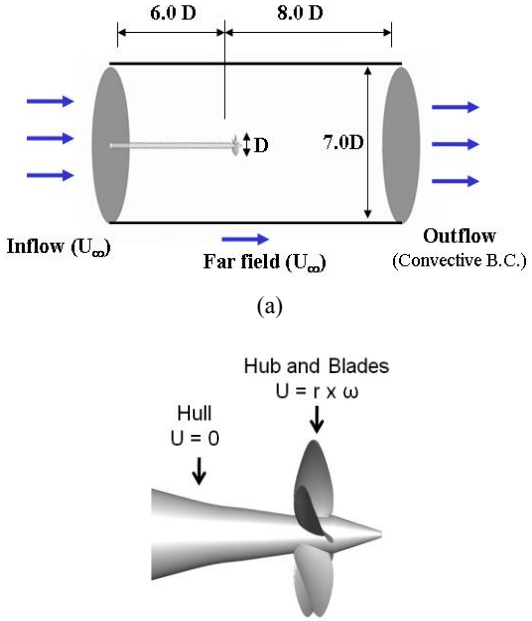

Figure 3. (a) Computational domain and boundary conditions on domain boundaries; (b) boundary conditions on solid walls (Fig. reproduced with permission from Verma et al. 2012).

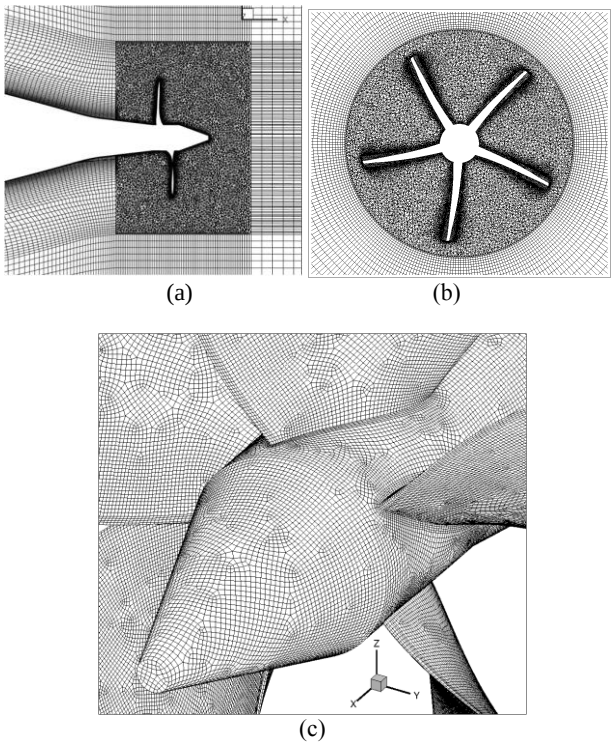

Figure 4. Computational grid: (a) xy plane; (b) x=0 plane; (c) surface mesh on the propulsor (Fig. reproduced with permission from Verma et al. 2012).

propulsor geometry and hub geometry are given in Jessup et al. (2006).

The computational domain is a cylinder with diameter 7.0D and length 14.0D where D is the diameter of the propulsor disk. Half body of the hull is used and stabilizing fins are ignored. Free-stream velocity boundary conditions are specified at the inlet and the lateral boundaries. Convective boundary conditions are prescribed at the exit. As mentioned, boundary conditions on solid walls are forced as those are prescribed in the inertial reference frame. Thus, boundary conditions on rotor part, blades and hub, are specified as $u = \omega \times r$, while no-slip boundary conditions are prescribed on the hull. A schematic of computational domain and boundary conditions is shown in Figure 3.

In the present work, simulations are performed for the propulsor with hull at J=-1.0 and J=-0.5. The computational grid used here has 7.3 million elements. Four layers of prisms with a minimum wall-normal spacing of 0.0017D and a growth ratio of 1.05 are extruded from propulsor surface which is paved with quadrilateral elements. The unstructured grid used in the simulation is shown in Figure 4.

3 Dynamic Mode Decomposition (DMD)

We perform DMD of the full three-dimensional velocity field. We store (m + 1) snapshots of the three velocity components at each spatial location and express the last snapshot as a linear combination of the previous snapshots. The size of each x_i vector is the number of grid points multiplied by the number of velocity components. The size of each vector is 7.3 million times 3 = 21.9 million for the hull-attached propeller. Let **K** represent a matrix of the different snapshots from $\mathbf{x}_0$ to $\mathbf{x}_{m-1}$,

$$\mathbf{K} = [\mathbf{x}_0, \mathbf{x}_1, \dots , \mathbf{x}_{m-1}] \tag{2}$$

Since each snapshot ($\mathbf{x}_i$) is obtained by applying the discrete Navier–Stokes operator (represented by the matrix **A**) to the previous snapshot ($\mathbf{x}_{i-1}$), the matrix **K** can also be written as:

$$\mathbf{K} = [\mathbf{x}_0, \mathbf{A}\mathbf{x}_0, \mathbf{A}^2\mathbf{x}_0, \dots , \mathbf{A}^{m-1}\mathbf{x}_{m-1}] \tag{3}$$

Now, expressing the last snapshot ($\mathbf{x}_m$) as a linear combination of the previous snapshots,

$$\mathbf{x}_m = c_0\mathbf{x}_0 + c_1\mathbf{x}_1 + \dots + c_{m-1}\mathbf{x}_{m-1} + \mathbf{r} = \mathbf{K}\mathbf{c} + \mathbf{r} \tag{4}$$

In the above equation, **r** represents the residual of the linear combination. If the matrix **A** were linear, then the above representation would be exact, thus making the residual zero. Since the Navier–Stokes operator is non–linear, there is a finite residual and the decomposition approximates the eigenvalues of the matrix **A**. Here, **c** is given by:

$$\mathbf{c} = (c_0, c_1, \dots , c_{m-1})^T \tag{5}$$

The vector **c** contains constants c_j, which are obtained by solving the Least-Squares problem in Equation 4 using Singular Value Decomposition (SVD). Based on the above definitions, we get:

$$\mathbf{A}\mathbf{K} = \mathbf{K}\mathbf{C} + \mathbf{r}\mathbf{e}^T , \mathbf{e}^T = (0, 0, \dots , 1) \tag{6}$$

where, **C** is a companion matrix whose eigenvalues approximate those of the matrix **A**, which represents the dynamics of the flow. The imaginary part of the eigenvalue gives the frequency while the real part gives the growth rate of the mode. The eigenvector (**v**) or the spatial variation of the DMD mode is obtained from the eigenvector of the companion matrix (**C**) and the matrix (**K**). The energy of each DMD mode is the L_2-norm of the eigenvector **v**. The reader is referred to Rowley et al. (2009) and Schmid (2010) for further details.

This algorithm has been validated (not shown here) for two-dimensional flow over a circular cylinder at Reynolds number (Re=DU/ ν) of 60, 100 and 200 by comparing the Strouhal number (St=fD/ U) obtained from DMD to the Strouhal number obtained from the time history of lift in the DNS.

4 RESULTS

Large-Eddy Simulations are performed under the crashback condition at two different negative advance ratios of J=-1.0 and J=-0.5 at Reynolds number Re = 480,000. The advance ratio J and Reynolds number *Re* are defined as

$$J = \frac{U}{nD}, \quad \mathrm{Re} = \frac{DU}{\nu} \tag{7}$$

where, U is the free-stream velocity, n is the propulsor rotational speed, D is the diameter of the propulsor disk and υ is the kinematic viscosity.

Thrust T is the axial component of force. Torque Q is the axial component of the moment of force. F_H and F_V are the horizontal and vertical projections of the force. Their vector sum is the projection of the force onto the direction perpendicular to the propulsor axis and is termed the side-force S. Since computations are performed in the rotating frame of reference, the side-force is translated to the inertial reference frame. The horizontal and vertical components of the side-force, F_H and F_V, respectively, can be obtained from a rotational transformation using the angle between the rotating frame and the inertial frame.

Non-dimensional thrust coefficient K_T, torque coefficient K_Q, and side-force coefficient K_S are given by,

$$K_T = \frac{T}{\rho n^2 D^4}, \quad K_Q = \frac{Q}{\rho n^2 D^5}$$
$$K_S = \frac{\sqrt{F_H^2 + F_V^2}}{\rho n^2 D^4} \tag{8}$$

where, ρ is the density of the fluid.

4.1 Description of flow field

Verma et al (2012) computed time averaged statistics of flow field for J=-1.0 and J=-0.5. XY plane cutting the center and along the length of the hull is shown along with time averaged pressure and velocity streamlines for J=-1.0 and J=-0.5 in Figure 5a and 6a respectively. The time averaged flow statistics are further averaged along lines of constant radius to yield circumferentially averaged statistics in the XR plane. Figure 5b and 6b shows contours of axial velocity with streamlines for circumferentially averaged statistics. The blanked out zone is where the hull/shaft and the propulsor blade would be.

Comparing the two cases of advance ratios, we observe that the recirculation zone, which is generated by the interaction of reverse flow due to propeller with the hull wake, is smaller and lies further upstream for lower negative advance ratio of J=-0.5. This happens because at lower negative advance ratio, the recirculation zone is suppressed by stronger reverse flow and pushed further upstream. Also, the ring vortex is seen closer to the propulsor disk at lower negative advance ratio of J=-0.5 compared to J=-1.0 case for the same reason.

Verma et al. (2012) also computed the power spectral density (PSD) of coefficient of side-force magnitude K_s for both advance ratios (Figure 7), which showed good agreement with the experimental results for propulsor with hull.The blade passage frequency of 5 rev^{-1} was observed as a peak for both advance ratios. Another peak was found at a lower frequency of f=0.16 rev^{-1} for the case of higher negative advance ratio of J=-1.0. This low-frequency, high-amplitude modulation of the side force affects the maneuverability of the marine vessel. Besides, the higher harmonics of blade passage frequency f=10, 15 rev^{-1} are also observed for J=-0.5 but with smaller amplitude in the PSD of side-force magnitude (Figure 7b). Interestingly, they also observed peaks at f= 1 rev^{-1} in the PSD spectra of side-force magnitude for propeller crashback without hull for both advance ratios (J=-1.0 and J=-0.5), which was not observed in the presence of hull.

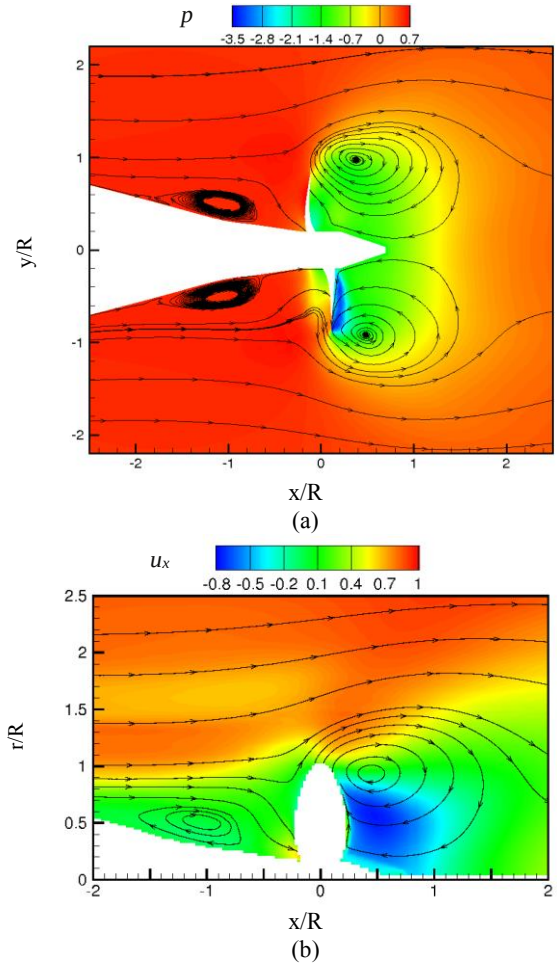

Figure 5. J=-1.0. Time-averaged flowfield (a) pressure contours with streamlines; (b) Circumferentially averaged axial velocity with streamlines (Fig. reproduced with permission from Verma et al. 2012).

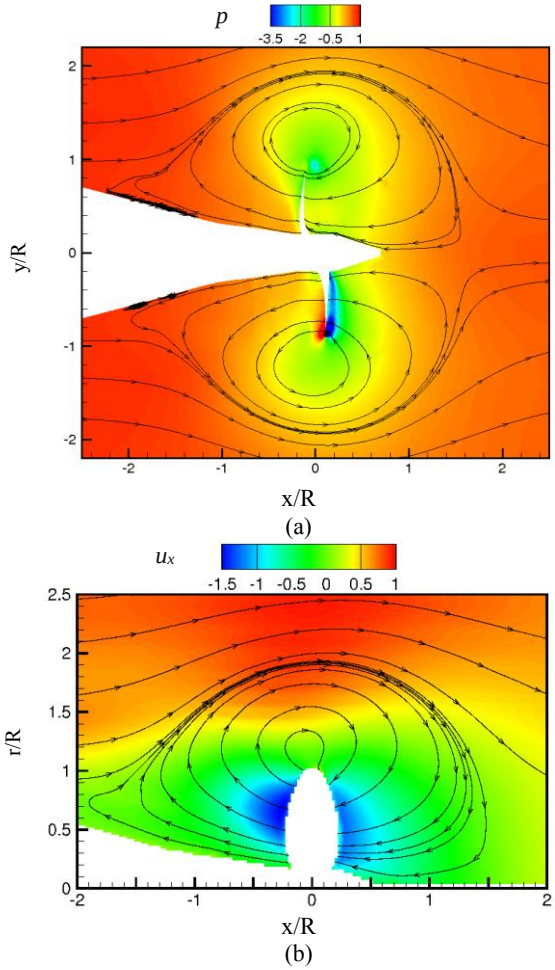

Figure 6. J=-0.5. Time-averaged flowfield (a) pressure contours with streamlines; (b) Circumferentially averaged axial velocity with streamlines (Fig. reproduced with permission from Verma et al. 2012).

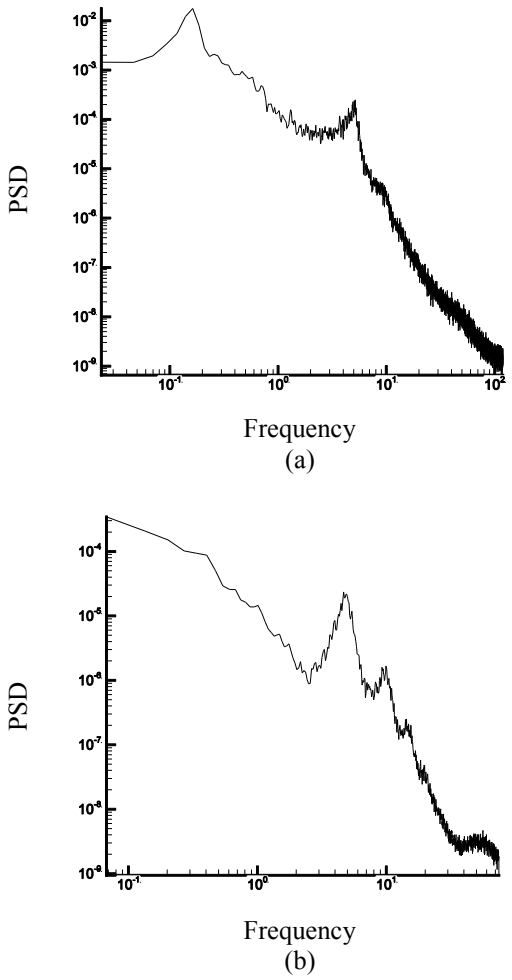

Figure 7. PSD of K_S: (a) J=-1.0; (b) J=-0.5.

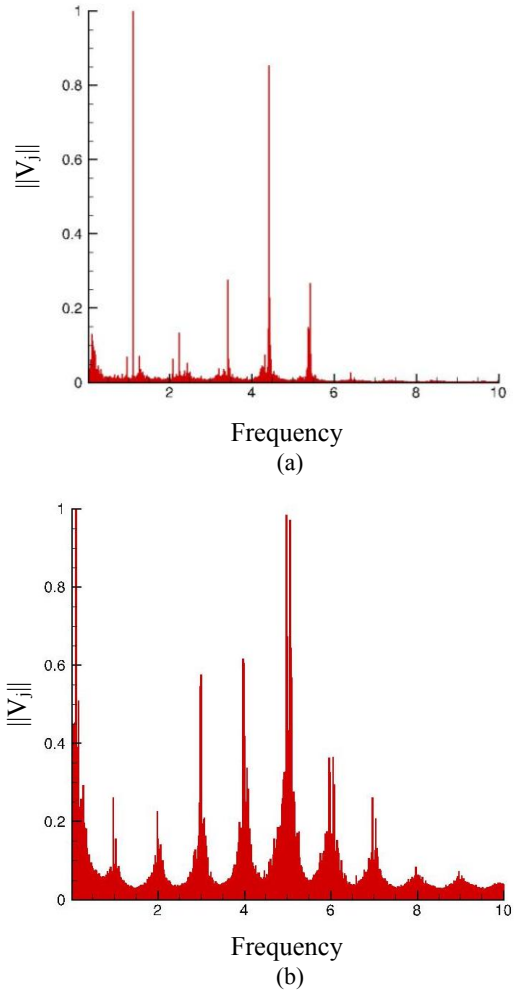

Figure 8. The magnitude of normalized DMD modes (except the first one): (a) J=-1.0; (b) J=-0.5.

4.2 DMD modes and frequencies

The spectra of side-force magnitude experienced by a hull-attached propeller have been described earlier. The side-force is an integral quantity which is related to the flow field. In order to understand the relation between the dominant frequencies in the side-force spectra and the flow structures, DMD of the three dimensional flow field is used. LES is performed for both advance ratios and 1200 snapshots of the velocity field are stored after the flow has converged statistically, which are then used in the algorithm described earlier in section 3. These 1200 snapshots spanned 60 rotations of the propeller with a temporal spacing of 0.05 rotation time (= tU / JD) between two successive snapshots. The first DMD (Koopman) mode is the time-averaged flow field which captures the steady flow structures and has the highest energy. All other eigenvalues occur in complex conjugate pairs and hence, only the positive frequencies are plotted and discussed here. The energy corresponding to each frequency is normalized by the energy of the highest energy mode. Figure 8 shows the normalized magnitude of DMD modes at each frequency for both cases of advance ratios. Each mode represents a flow structure that oscillates with one single frequency and the superimposition of several such modes results in the quasi-periodic global system.

Comparing the DMD spectra, we notice that the most important difference between the two cases, is the existence of a distinct peak at f=1.11 rev^{-1} for J=-1.0 case. The axial velocity contour for this low-frequency mode at J=-1.0 is plotted in Figure 9. This low-frequency mode features large-scale positive and negative axial velocity which is shed downstream in the wake. The length scale of flow structures seems to grow as we move further downstream. The high-frequency mode is susceptible to noise and also sensitive to grid resolution. The noise is reduced by splitting the total number of samples into 4 non-overlapping group of

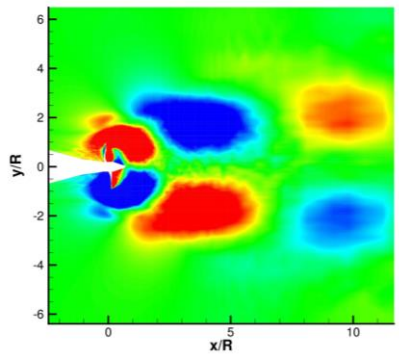

(a)

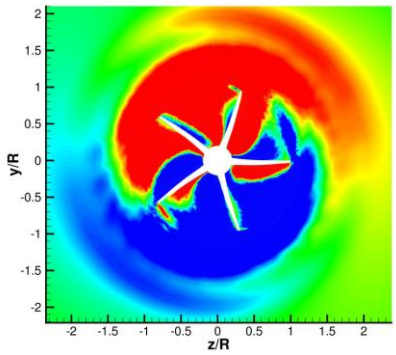

(b)

Figure 9. J=-1.0, axial velocity contour for the DMD mode at f=1.11 rev^{-1}; (a) xy plane; (b) x=0 plane.

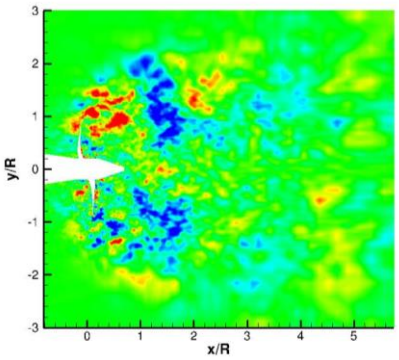

(a)

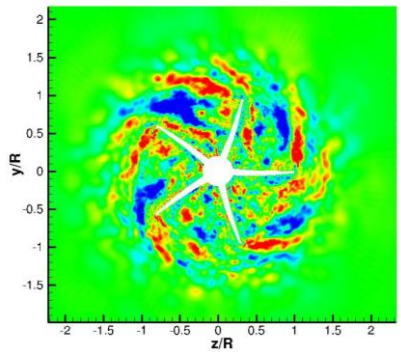

(b)

Figure 10. J=-1.0, axial velocity contour for the DMD mode at 4.42 rev^{-1}; (a) xy plane; (b) x=0 plane.

snapshots each and averaging the DMD spectra. Figure 10 shows the dominant high-frequency mode of f=4.42 rev^{-1} for J=-1.0. This mode has smaller scales compared to the low-frequency mode described earlier.

The DMD spectra for J=-0.5 lack the distinct low-frequency peak. Instead, the energy seems spread across all the integral frequencies. The dominant frequency which occur at f=5 rev^{-1} is analyzed here. The mode corresponding to this dominant frequency at J=-0.5 is plotted in Figure 11. This mode looks significantly different than the high-frequency mode for J=-1.0 case discussed earlier. As seen in the xy plane (Figure 10a & 10b), the flow structures seem to be further upstream for lower negative advance ratio of J=-0.5. This seems to be the consequence of stronger reverse flow at J=-0.5.

The high-frequency mode seems to capture the flow structures that are formed when the rotating propulsor cuts the incoming wake of the hull. One point to note here is that since we have used flow field snapshots spanning only 60 propulsor rotation time for both advance ratios, very low frequencies (say the peak observed at f=0.1 rev^{-1}) are not analyzed here.

We may expect the peaks in the DMD spectra to match with that of side-force PSD spectra closely. But we observe that the location of the peaks is different. This is because the DMD spectra show distribution of energy across various frequencies in the entire domain whereas the side-force magnitude on the body is affected by the flow field in the vicinity of the body.

To completely understand the relation between the unsteady loads and the corresponding flow features, we need to analyze DMD spectra of propeller crashback in the absence of hull where there is no wake of hull and hence the upstream recirculation zone is absent. DMD of pressure field can also be used to get insight into the side-force generation mechanism. Moreover, in order to make sure that 1200 snapshots of flow field are sufficient for DMD, a convergence study of the residual norm needs to be done by showing that the residual norm does not change with more number of samples. All of these are work in progress.

5 Summary

LES of propulsor is performed in the presence of upstream hull at negative advance ratios of J=-1.0 and J=-0.5 (similar to Verma et al. 2012), which lie on the either side of critical advance ratio J=-0.7 beyond which a hull is known to drastically increase side-force magnitude. 1200 snapshots of

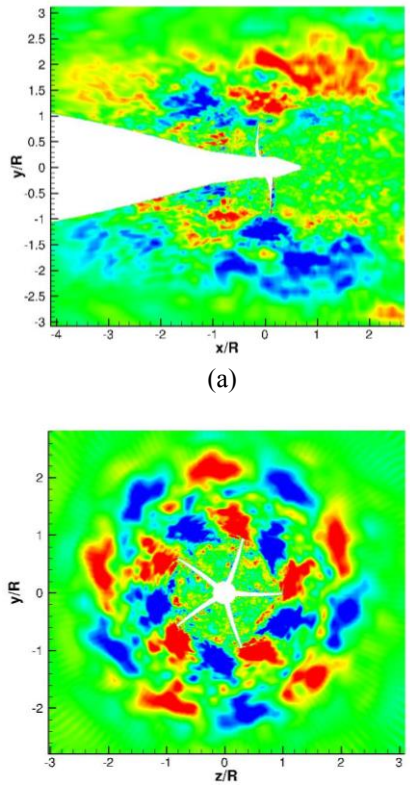

Figure 11. J=-0.5, axial velocity contour for the DMD mode at f=5 rev^{-1}: (a) xy plane; (b) yz plane.

velocity field with a temporal spacing of 0.05 rotation time (= tU / JD) between two successive snapshots are stored after the flow has converged statistically for both advance ratios of J=-1.0 and J=-0.5. DMD of three-dimensional velocity fields is performed to extract the dominant frequencies and corresponding modes for both the cases. Each DMD mode by construction, represents one particular frequency and hence, is very effective in isolating the complex dynamics of a complicated system. The basic idea is to identify and analyze the dominant flow features to have better understanding of flow physics leading to the development of reduced-order model for propeller crashback.

The analysis of the results reveal the presence of a distinct dominant low-frequency mode at f=1.11 rev^{-1} for higher negative advance ratio (J=-1.0). This mode shows large-scale flow features growing in size as we move downstream of the propeller. A dominant high-frequency mode is also observed at f=4.42 rev^{-1} and f=5 rev^{-1} for J=-1.0 and J=-0.5 respectively. This high-frequency mode has smaller scale flow structures. The main difference between the high-frequency modes of the two advance ratios is that the flow structures are located further upstream for lower negative advance ratio (J=-0.5). This happens due to stronger reverse flow at lower negative advance ratio (J=-0.5). The low-frequency mode seems to capture the flow structures in the hull wake (recirculation zone) when the reverse flow due to propeller is weaker (J=-1.0). Stronger reverse flow due to propeller suppresses the flow structures in the hull wake and hence, this dominant mode is not observed for lower negative advance ratio (J=-0.5). The high-frequency mode captures the flow structures formed when the rotating propulsor cuts the wake of hull.

In conclusion, the crashback flow over propulsor in the presence of hull has two main flow features- a ring vortex and an upstream recirculation zone. The location and strength of the upstream recirculation zone and the ring vortex depends on the advance ratio J, which characterizes the relative strength of the reverse flow in comparison with the incoming freestream. The presence of hull affects the unsteady loads experienced by the propulsor and the extent of hull's effect depends on the advance ratio. Both these flow features, recirculation zone and ring vortex, may have more than one frequency. The unsteady loads experienced by the propulsor depends on the dynamic interaction of the recirculation zone with the ring vortex. The development of a reduced-order model needs proper understanding of the dynamics of the flow system. The exact relation between the DMD modes and the unsteady loads on the body needs further investigation.

ACKNOWLEDGEMENTS

This work was supported by the United States Office of Naval Research under ONR Grant N000141410289 with Dr. Ki-Han Kim as technical monitor. Computing resources were provided by the Arctic Region Supercomputing Center of HPCMP and the Minnesota Supercomputing Institute. The authors acknowledge Dr. Aman Verma and Dr. Prahladh Iyer for valuable discussions and comments.

REFERENCES

Bagheri, S. (2010), "Koopman-mode decomposition of the cylinder wake", Journal of Fluid Mechanics, Vol. 726, pp. 596-623.

Bridges, D.H., (2004), "A detailed Study of the Flowfield of a Submarine Propeller During a Crashback Maneuver", Aerospace Engineering, Mississippi State University, Report No. MSSU-ASE-04-1.

Chang, P., Mahesh, K. (2006), "Large Eddy Simulation of Crashback in Marine Propulsors", Proceedings of the 26th Symposium on Naval Hydrodynamics, Rome.

Chen, B., Stern, F. (1999), "Computational Fluid Dynamics of Four Quadrant Marine Propulsor Flow", Journal of Ship Research, Vol. 43, No. 4, pp. 218-228.

Davoudzadeh, F., Taylor, L. K., Zierke, W. C., Dreyer, J. J., McDonald, H., Whitfield. D. L. (1997), "Coupled Navier-Stokes and Equations of Motion Simulation of

Submarine Maneuvers, Including Crashback", Proceedings of the 1997 ASME Fluids Engineering Division Summer Meeting, Vol. 2, New York.

Germano, M., Piomelli, U., Moin, P., Cabot, W. H. (1991), "A dynamic Subgrid-Scale Eddy Viscosity Model", Physics of Fluids A, Vol. 3, No. 7, pp.

Holmes, P., Lumley, J. L. & Berkooz, G. (1996), "Turbulence, Coherent Structures, Dynamical Systems and Symmetry", Cambridge University Press.

Jang, H., Mahesh K. (2013), "Large Eddy Simulation of flow around a reverse rotating propeller", Journal of Fluid Mechanics, Vol. 729, pp. 151 – 179.

Jiang, C. W., Dong, R. R., Lui, H. L., Chang, M. S. (1997), "24-inch Water Tunnel Flow Field Measurements During Propulsor Crashback", 21st Symposium on Naval Hydrodynamics, The National Academies Press, Washington DC, pp. 136-146.

Jessup, S., Chesnakas, C., Fry, D., Donnelly, M., Black, S., Park, J. (2004), "Propulsor Performance at Extreme Off Design Conditions", Proceedings of the 25th Symposium on Naval Hydrodynamics, Canada.

Jessup, S., Fry, D., Donnelly, M. (2006), "Unsteady Propulsor Performance in Crashback Conditions With and Without Duct", Proceedings of the 26th Symposium on Naval Hydrodynamics, Rome, Italy.

Lilly, D. K. (1992), "A Proposed Modification of the Germano Subgrid-Scale Closure Model", Physics of Fluids A, Vol. 4, No. 3, pp. 633-635.

Mahesh, K., Constantinescu, G., Moin, P. (2004), "A Numerical Methods for Large-Eddy Simulation in Complex Geometries", Journal of Computational Physics, Vol. 197, No. 1, pp. 215-240.

Mezić, I. (2013), "Analysis of Fluid Flows via Spectral Properties of the Koopman Operator", Annu. Rev. Fluid Mech. 45:357-78.

Rowley, C.W., Mezić, I., Bagheri S., Schlatter,P., Henningson, D. S. (2009), "Spectral analysis of nonlinear flows", Journal of Fluid Mechanics, Vol. 641, pp. 115-127.

Schmid, P. J. (2010), "Dynamic mode decomposition of numerical and experimental data", Journal of Fluid Mechanics, Vol. 656, pp. 5-28.

Verma, A., Jang, H., Mahesh, K. (2012), "The effect of an upstream hull on a propeller in reverse rotation", Journal of Fluid Mechanics, Vol. 704, pp. 61-88.

Vyšohlíd, M., Mahesh, K. (2006), "Large Eddy Simulation of Crashback in Marine Propulsors", Proceedings of the 26th Symposium on Naval Hydrodynamics, Rome.

DISCUSSION

Question from Tobias Huuva

What did you mean by variable pitch? Will your refinement box influence the vortex?

Authors' Closure

Thank you for your questions. The propeller used in our simulations (P4381) is a variable-pitch propeller in radial direction but the pitch is fixed. (See Jessup et al., 2004, 2006) Also, the refinement box around the propeller is filled with tetrahedral cells everywhere except 4 layers of prisms, which grow out of propeller surface as described in section 2.2 of this paper. As the flow is massively separated in this region, the used grid resolution was found sufficient for resolving the essential flow features. Thus, the refinement box doesn't influence the vortex in our experience.

Question from Antoine Ducoin

Your Dynamic Mode Decomposition is performed with a high number of snapshots. What is the influence of number of snapshots on your mode resolution? In my opinion, increasing the number of snapshots could lead to possible noises in the spatial distribution of your mode.

Authors' Closure

Thank you for your question. Increasing the number of snapshots beyond a certain limit can indeed increase noise in spatial distribution of modes. Using singular value decomposition (SVD) as a preprocessing step to data sequence helps in reducing such noise. Please see Schmid (2010) for details.